PATIENT-SPECIFIC AORTIC VALVE BLOOD FLOW SIMULATIONS

Scott Kulp[1]*, Zhen Qian*[2]*, Mani Vannan*[2]*, Sarah Rinehart*[2]*, Dimitris Metaxas*[1]

[1]CBIM Center, Rutgers University, Piscataway, NJ 08854, USA
[2]Piedmont Heart Institute, Atlanta, GA 30309, USA

ABSTRACT

In this paper, we present a novel framework to simulate and visualize blood flow at high levels of detail through the aortic valve. We generate a 4D reconstruction of the aortic root using contrast-enhanced CT imagery, and attach it to a model of the left ventricle segmented from the Visible Human Project dataset. This full R-R animated model is then used as solid boundary conditions in a highly-accurate FDM Navier-Stokes fluid solver. We perform this simulation on both healthy and diseased aortic hearts, and then build visualizations of the velocity and vorticity fields produced by the simulator. In our quantitative analysis of the flow, we find significantly elevated vorticities in the diseased valve simulation. These results produce a view of the flow fields clearer than previous imaging techniques can provide.

Index Terms— Blood flow, aortic valve, CT

1. INTRODUCTION

Aortic valve disease-induced alterations in the blood flow pattern may promote chronic remodeling of the aortic root and the left ventricle. Although the mechanism of the aortic root remodeling is not fully understood, the hemodynamic pattern in the aortic valve vicinity is believed to play an important role. Color Doppler echocardiography and MR phase-contrast flow imaging are two clinical techniques used in quantifying valvular blood flow [1, 2]. However, both techniques are limited in imaging the blood flow in the aortic valve vicinity. Color Doppler echocardiography is not suitable for 3D flow velocity quantification because of the one dimensional imaging angle. MR flow imaging has a limited 3D spatial resolution that makes it difficult to quantify a high-resolution flow pattern in a small structure of the aortic root. Furthermore, the blood flow in the aortic vicinity exhibits high rates of acceleration and a turbulent pattern with high vorticity, which compromises the flow quantification accuracies of Doppler-based echocardiography and phase-contrast MRI. In [3] , it is found that the aortic flow quantification discrepancy found in color Doppler echocardiography and phase-contrast MRI mainly came from the flow vorticity.

In this paper, we propose a framework to study the blood flow within the aortic valve vicinity using the computational fluid simulation and patient-specific aortic root models. Computational fluid simulation has been employed in the studies of the intraventricular flow and aortic flow. In 2011, Kulp et al [4] described a method of extracting the heart and its motion from CT to capture the geometry of the trabeculae and papillary muscles and show evidence of interactions between these structures and the blood flow. On the other hand, CT has become an important preprocedural imaging tool for assessing the aortic root anatomy in transcatheter aortic valve implantation patients, because of its high spatial resolution and high reproducibility [5]. In this study, we utilized CT as the imaging modality for accurate aortic valve modeling.

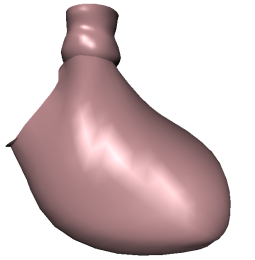

Fig. 1. Our aortic root model is attached to the left ventricle model segmented from Visible Human Project data to form a complete system of the left ventricle, the left ventricle outflow tract, and the aortic root.

Our paper is organized as follows: In Section 2, we describe our methodology for generating the 3D aortic root models from high-resolution CT data, as well as our method of applying inflow boundary conditions to the valve. In Section 3, we discuss the fluid simulation system we use to solve the Navier-Stokes equations and solve the fluid flow across the valve. In Section 4, we show our results and visualizations of the blood flow simulations on both healthy and diseased aortic valve. Finally, in Section 6, we present our conclusions and discuss our future work.

2. DATA ACQUISITION

The aortic root models were reconstructed from contrast-enhanced 3D CT images that were acquired using a retrospective full R-R ECG gating protocol. In each heart cycle, 10 phases of 3D CT volumes were reconstructed at every 10% interval. The patient-specific aortic models were semi-automatically reconstructed using a valve segmentation research software (Siemens Cooperate Research). The aortic

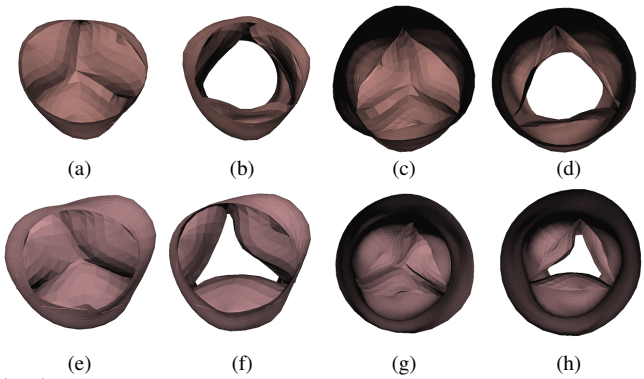

Fig. 2. Four views each of both our healthy (top) and stenotic (bottom) aortic root models reconstructed from CT data.

models of the 10 temporal phases were further aligned and registered to generate a smooth aortic root motion model. Images of the stenotic valve can be seen in Figure 2.

In addition to the geometry and motion of the valve, inflow boundary condition plays a critical role in determining the accuracy of our simulation results. However, the inflow boundary condition is largely determined by the left ventricular function. We cannot use patient-specific left ventricle geometries in this work, as we are focused solely on the impact of valvular geometry and motion on the aortic flow patterns, independent of changes in LV function. Therefore, we attach our aortic root models to a standard 3D model of a human left ventricle, which was reconstructed from the high-resolution Visible Human Project datasets, as discussed by Hurmusiadis et al [6]. Ventricular motion was derived from a fiber-based deformation model, also described in [6]. Models generated using this method were used in [7] to simulate flow through the left ventricle with high accuracy, so we are confident that these models provide acceptable inflow velocity boundary conditions to the aortic root. We removed the aortic root structures generated from the Visible Human Project data, and manually attached our own reconstructed aortic root models, as seen in Figure 1. We then used this full, animated model as the solid boundary conditions in our fluid simulator, as described below.

3. FLUID SIMULATION

The motion of an incompressible fluid is governed by the laws of conservation of momentum and mass, modeled by the Navier-Stokes (NS) equations:

$$\rho(\tfrac{\partial u}{\partial t} + u \cdot \nabla u) = -\nabla P + \mu \nabla^2 u,$$
$$\nabla \cdot u = 0.$$

Here, ρ is the fluid density, u is the 3D velocity vector field, P is the pressure field, and μ is the coefficient of viscosity. We seek to solve these equations for velocity and pressure.

Foster and Metaxas [8] were the first to develop a fast method of solving the NS equations for graphics applications by applying a staggered grid across the domain and explicitly solving for velocity at the cell faces. They then used successive over-relaxation to solve for pressure and correct the velocities to maintain incompressibility.

Our fluid-solid interaction system uses a "boundary immersed in a Cartesian grid formulation", allowing for an simple treatment of complex moving geometries embedded in a closed computational domain. In 2005, Yokoi et al. [9] applied the formulation of Sussman [10] to both graphics and medical simulations. More recently, Zelicourt et al. [11] implemented a similar system that can efficiently deal with complex geometric data, such as a system of blood vessels.

The heart models used here are embedded in a computational mesh of 100^3 cells on which the full NS equations are solved using FDM. The blood is modeled as a Newtonian fluid, with viscosity of 4mPa· s and density of 1050kg/m^3, which are physiologically accepted values for normal human blood[12]. The heart model is given to the solver as a set of meshes with point correspondences, which allows for easy interpolation and also obtaining the velocity of the heart mesh at every point in time. Our system represents the 3D meshes as a Marker Level Set(MLS) [7], where markers are placed on the boundary and are used to correct the level set at every time step. Since markers are only placed on the surface, MLS has been proven to be more efficient and more accurate for complex boundaries. The MLS and its velocity are rasterized onto the Eulerian grid and are used to impose the appropriate boundary conditions in the fluid solver. A simulation of a single cardiac cycle takes about 16 hours to complete on a machine with an Intel i7 processor and 16GB of RAM.

4. VISUALIZATIONS

After solving the flow fields for both aortic root models, we then use Paraview to visualize the results. We are primarily focused on differences in flow velocity and vorticity between the healthy and diseased valves. Our methods for visualization are described below.

Figure 3 gives visualizations of the velocity field of both valve models at two different time steps. Fluid velocity is represented by cones pointing in the direction of the flow and we change the hue of a cone depending on the magnitude of velocity at its location. At hue=160 (blue), velocity is approximately 3.5cm/s, and at hue=0 (red), velocity is approximately 190cm/s. Areas of flow velocities less than 3.5cm/s are not shown in our renders, as they tend to be noisy and less interesting in our analysis. Figures 3 (a) and (b) show the flow field through the healthy aortic valve in early and late systole, respectively, while figures 3 (c) and (d) give the flow field through the diseased aortic valve, also in early and late systole, respectively. To provide a more useful comparison, Figures 3 (a) and (c) were taken exactly the same time step and at the same angle, as were Figures 3 (b) and (d).

In Figure 4, we have visualizations of the flow vorticity at several time steps. Since vorticity is a scalar field, we render it volumetrically, rather than in the glyph-based manner of the

velocity field. Similar to Figure 3, the color of a particular region represents the magnitude of the vorticity at that point. At hue=160 (blue), vorticity is nearly $0s^{-1}$, and at hue=0 (red), vorticity is approximately $3s^{-1}$. Like Figure 3, Figures 4 (a) and (b) are of the healthy aortic valve, while (c) and (d) are of the diseased valve. Each image in Figure 4 was taken at the same time step and at the same angle as their respective images in Figure 3.

Finally, Figure 5 include images of plotted streamlines in late systole through the healthy and diseased valves. Colors represent velocity magnitude at a given point in the streamline, and are scaled in precisely the same way as in Figure 3. This image was taken at the same timestep as in Figures 3 (b)/(d) and Figures 4 (b)/(d).

5. RESULTS AND DISCUSSION

From Figures 3-5, we can see that this simulation framework provides a very clear view of the flow fields in both of our experiments. In our streamline visualization, Figure 5, we see the formation of vortices in detail. Vortices are also easily visible in the velocity fields of Figure 3, especially in the diseased valve case, and in late systole. In Figure 6 (a), we compute the average velocities through both the diseased and healthy valves at the sino-tubular junction. The time steps plotted were temporally equally spaced, and in every time step, both valves were open. We can see that in early systole, flow through the aorta in both simulations had very similar velocities. However, in mid-late systole, flow in the aorta appears to drop more rapidly in our diseased valve simulation, showing the decreased efficiency of the stenotic aortic valve.

In Figure 4, the vorticity fields strongly agree with our findings in the previous images. In the sinus region, we note the high rotational energy against the stenotic valve, as compared to the healthy valve, which is consistent with the vortices visible in the streamlines and velocity field. We also note that regions of elevated vorticity are visible in both simulations at the regions above the sinus, especially in late systole. In Figure 6 (b) we have plotted mean vorticities during systole at the sinus and above-sinus regions. Only those points at least one full grid cell away from the wall were included in the mean vorticity computation. We see that the flow through the stenotic valve consistently produces mean vorticities significantly higher than the healthy valve in both regions. Interestingly, in the diseased case, vorticities seem to slightly grow through time in the region above the sinus, and decrease in the sinus region. This is possibly due to the effects of flow separations and shedding vorticies. This is also seen more dramatically with the healthy valve in the final plotted time step, with voriticites in the segment above the sinus sharply increasing, while decreasing at the sinus. Again, we hypothesize that this is due to vortex shedding caused by the valve beginning to close.

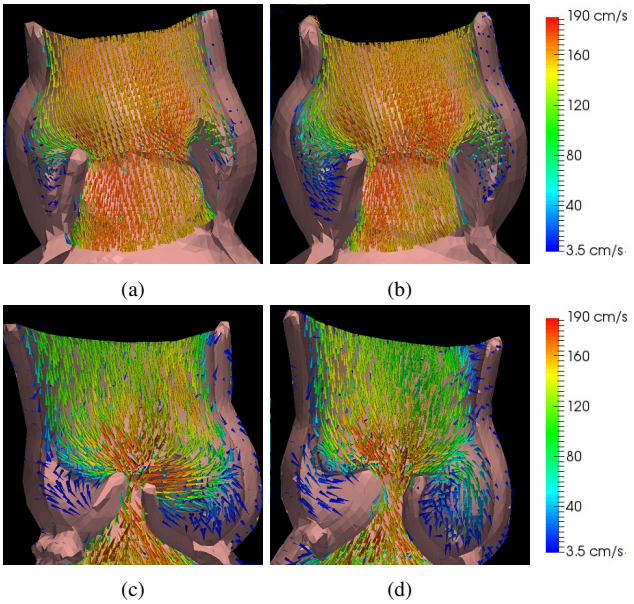

Fig. 3. Velocity field visualizations. (a) Early systole, healthy valve; (b) Late systole, healthy valve; (c) Early systole, diseased valve; (d) Late systole, diseased valve. Both (a) and (c) were taken at the same time step, as were (b) and (d)

6. CONCLUSIONS AND FUTURE WORK

In this paper, we have presented a new framework to simulate and visualize blood flow through patient-specific aortic root models. Our results provide a clear, high-resolution view of flow patterns, which have been previously not visible in traditional flow imaging techniques, such as Doppler-based echocardiography and phase-contrast MR. We clearly can see differences in flow patterns through normal and abnormal aortic valve geometries and motion, which could potentially become a highly useful tool for doctors and scientists to assist in diagnosis and understanding valvular diseases.

In the future, we plan on improving this framework in several ways. Currently, while LV motion can be adjusted to replicate certain defects, such as hypokinesis, it would be optimal to use models of the patient's true LV by segmenting CT/MRI images of their full heart. This way, our framework would be fully patient-specific, including inflow boundary conditions to the aortic root.

7. ACKNOWLEDGMENTS

This work is supported by the Multiscale Quantification of 3D LV Geometry from CT project, sponsored by NHLBI under Grant Award Number 5R21HL088354-02.

8. REFERENCES

[1] Bonow, RO. and Carabello, BA. and Chatterjee, K. and et al, "2008 Focused update incorporated into the ACC/AHA 2006 guidelines for the management of patients with valvular heart disease: a report of the American College of Cardiol-

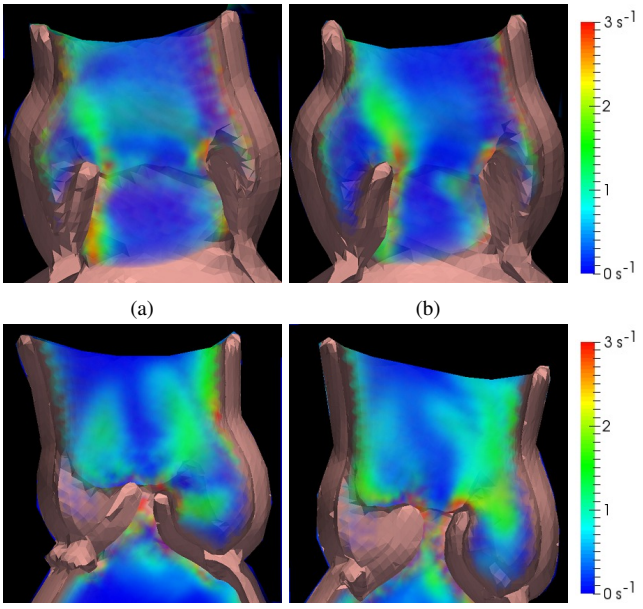

Fig. 4. Vorticity field visualizations. (a) Early systole, healthy valve; (b) Late systole, healthy valve; (c) Early systole, diseased valve; (d) Late systole, diseased valve. Each image was taken at the same time step as their corresponding images in Figure 3

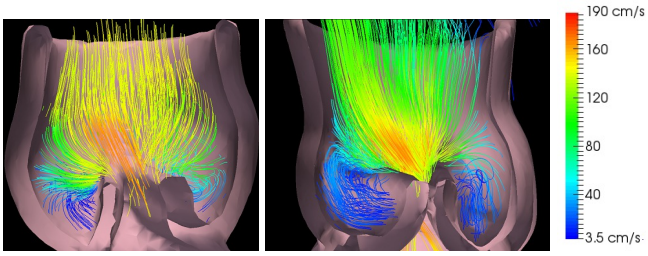

Fig. 5. Streamline visualizations of (a) healthy and (b) diseased aortic valve, late systole. Flow vortices are clearly visible.

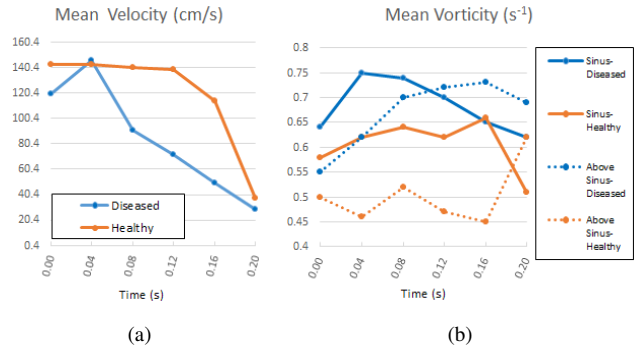

Fig. 6. Analysis of blood flow velocity and vorticity. (a) Mean velocity at the sino-tubular junction (b) Mean vorticity in sinus and above-sinus regions

ogy/American Heart Association task force on practice guidelines," *Circulation*, vol. 118, pp. e523–e661, 2008.

[2] Caruthers, SD. and Lin, SJ. and Brown, P. and Watkins, MP. and Williams, TA. and Lehr, KA. and Wickline, SA., "Practical value of cardiac magnetic resonance imaging for clinical quantification of aortic valve stenosis: comparison with echocardiography," *Circulation*, vol. 108, pp. 2236–2243, 2003.

[3] Garcia, J. and Capoulade, R. and Le Ven, F. and Gaillard, E. and Kadem, L. and Pibarot, P. and Larose, E., "Discrepancies between cardiovascular magnetic resonance and Doppler echocardiography in the measurement of transvalvular gradient in aortic stenosis: the effect of flow vorticity," *J Cardiovasc Magn Reson.*, vol. 15, no. 1, pp. 84, Epub ahead of print, Sept. 2013.

[4] Scott Kulp and Mingchen Gao and Shaoting Zhang and Zhen Qian and Szilard Voros and Dimitris N. Metaxas and Leon Axel, "Using high resolution cardiac ct data to model and visualize patient-specific interactions between trabeculae and blood flow.," in *MICCAI 2011*, 2011, pp. 468–475.

[5] Gurvitch, R. and Webb, JG. and Yuan, R. and Johnson, M. and Hague, C. and Willson, AB. and Toggweiler, S. and Wood, DA. and Ye, J. and Moss, R. and Thompson, CR. and Achenbach, S. and Min, JK. and Labounty, TM. and Cury, R. and Leipsic, J., "Aortic annulus diameter determination by multidetector computed tomography: reproducibility, applicability, and implications for transcatheter aortic valve implantation," *JACC Cardiovasc Interv.*, vol. 4, no. 11, pp. 1235–45, Nov. 2011.

[6] Hurmusiadis, Vassilios and Briscoe, Chris, "A functional heart model for medical education," in *Functional Imaging and Modeling of the Heart*, Frangi, AlejandroF. and Radeva, PetiaI. and Santos, Andres and Hernandez, Monica, Eds., vol. 3504 of *Lecture Notes in Computer Science*, pp. 85–91. Springer Berlin Heidelberg, 2005.

[7] Viorel Mihalef and Dimitris Metaxas and Mark Sussman, "Textured liquids based on the marker level set.," *Comput. Graph. Forum*, vol. 26, no. 3, pp. 457–466, 2007.

[8] Nick Foster and Dimitris Metaxas, "Realistic animation of liquids," *Graph. Models Image Process.*, vol. 58, pp. 471–483, September 1996.

[9] Kensuke Yokoi and Feng Xiao and Hao Liu and Kazuaki Fukasaku, "Three-dimensional numerical simulation of flows with complex geometries in a regular cartesian grid and its application to blood flow in cerebral artery with multiple aneurysms," *Journal of Computational Physics*, vol. 202, no. 1, pp. 1 – 19, 2005.

[10] Sussman, Mark, "A parallelized, adaptive algorithm for multiphase flows in general geometries," *Comput. Struct.*, vol. 83, no. 6-7, pp. 435–444, 2005.

[11] Diane de Zelicourt and Liang Ge and Chang Wang and Fotis Sotiropoulos and Anvar Gilmanov and Ajit Yoganathan, "Flow simulations in arbitrarily complex cardiovascular anatomies - an unstructured cartesian grid approach," *Computers & Fluids*, vol. 38, no. 9, pp. 1749 – 1762, 2009.

[12] Mihalef, Viorel and Ionasec, Razvan and Wang, Yang and Zheng, Yefeng and Georgescu, Bogdan and Comaniciu, Dorin, "Patient-specific modeling of left heart anatomy, dynamics and hemodynamics from high resolution 4d CT," in *ISBI*, Wiro Niessen and Erik Meijering, Eds., 2010, pp. 504–507.